The Eurasia Proceedings of Science, Technology, Engineering & Mathematics (EPSTEM)
ISSN: 2602-3199

The Eurasia Proceedings of Science, Technology, Engineering & Mathematics (EPSTEM), 2023

Volume 24, Pages 101-109

IConTech 2023: International Conference on Technology

PV Supplied Electrochemical Production of Hydrogen Peroxide: A Green Pathway for Fenton Based Advanced Oxidation Processes

Kaouther Kerboua
National Higher School of Technology and Engineering

Abstract: Hydrogen peroxide is the common reagent of the Fenton Based advanced oxidation processes, it is generally added in stochiometric yields to the Fenton catalyst (Ferrous or ferric ions) to produce hydroxyl radicals. In the present study, a green technique for the in-situ production of hydrogen peroxide is examined numerically, using modelling and simulation, based on PV supplied electrochemical process and carbon-based electrodes. The PV supply model is based on Maximum Power Point Tracking using ET-Solar M53640 panel, while the modelling of the performance of the electrochemical cell is based on an electrical equivalent schema of activation, ohmic, and concentration resistances. Two production pathways of hydrogen peroxide under acidic conditions are considered, namely the reduction of O_2 and the oxidation of H_2O. The performed simulations under 3 scenarios of solar radiation (low, middle and high) demonstrated that 300 W/m^2 of incident global radiation results in 0.35 A of feeding current, against 0.88 A under 600 W/m^2 and 1.41 A under 900 W/m^2. Simulations for hydrogen peroxide production under the three scenarios have been compared based on the O_2 reduction pathway, which is proved to be more performant, especially with the lower H_2O_2 cathodic decomposition.

Keywords: Simulation, PV supply, Fenton, Hydrogen peroxide, Model, Production.

Introduction

Advanced oxidation processes AOPs are nowadays recognized as the key solution for the tertiary treatment of wastewater, aiming at eliminating the recalcitrant pollutant from liquid effluents. The integration of AOPs as tertiary treatment techniques in the autonomous stations of onsite treatment of wastewater for irrigation is expected to be the future solution for providing safe and sufficient quantities of water to smallholding farmers adapted to all the type of cultures, particularly in lockdown areas. The efficiency of AOPs is related to the non-selective and highly reactive $^{\bullet}$OH radicals (Haag, 1992), which area chemical species of great interest in terms of degradation of organic pollutants and recalcitrant contaminants in aqueous solutions (Madhavan et al.,2010; Pawar & Gawande, 2015). Fenton-based techniques are ones of the most important classes of AOPs which use the decomposition of hydrogen peroxide in the presence of ferrous ions to produce hydroxyl radicals, while Fe(II) oxidizes to Fe(III),. However, these processes require a stoichiometric amount of hydrogen peroxide and the catalyst, Fe(II) (Andreozzi et al., 2000). Fe(III) is expected to regenerate Fe(II) through the reaction with hydrogen peroxide. However, this reaction is known to be very slow, owing to the formation of intermediate non-radical species such as $Fe(HO_2)^{2+}$. Consequently, the Fenton process needs high amounts of Fenton's reagent to generate a high enough quantity of $HO^{\bullet}$.

The present paper suggests a solar based technique for the in-situ production of hydrogen peroxide, in parallel to the in-situ production of Fenton's catalyst using the Galvano-Fenton technique. The integrated process is composed of an electrochemical cell supplied by a PV solar panel, and of carbon-based cathode and nickel anode, and a galvanic cell made of iron waste based anode and copper cathode. The process is modelled numerically from the solar supply to the chemical kinetics of Fenton's reaction initiated by the in situ produced

hydrogen peroxide and ferrous ions. The simulations are performed considering three scenarios of global solar radiation, namely 300, 600 and 900 W/m^2

Method

Configuration of the Process and Numerical Model

The modelled process is a combination of a PV supplied electrochemical cell for hydrogen peroxide production in acidic conditions, and a Galvanic cell for the spontaneous production of ferrous iron, as described in Fig.1. The electrochemical cell is designed using carbon based cathode and nickel anode, while the galvanic cell couples a sacrificial anode made of iron waste and a cathode of copper. Both cells are immersed within an acidic electrolyte that consists of an acqeous solution of sulfuric acid at pH 3. This pH allows the formation of ferrous ions according to the Pourbaix diagram, and favors the cathodic reduction of oxygen in the presence of hydrogen ions. Both reactions are shown respectively in Eqs.1 and 2.

$$\mathrm{Fe} \rightarrow \mathrm{Fe}^{2+} + 2\mathrm{e}^- \quad (1)$$

$$O_2 + 2\,H^+ + 2e^- \rightarrow H_2O_2 \quad (2)$$

In order to ensure a sufficient yield of oxygen at the cathode of the electrochemical cell, pure oxygen is continuously pumped into the electrolyte, the electrolyte is then permanently saturated with oxygen, whose concentration is described by the below Eq.3 (Tromans, 1998).

$$c_{O_2} = P_{O_2}\left(\frac{0.046\,T^2 + 203.357\,T\,Ln\left(\frac{T}{298}\right) - (299.378 + 0.092T)(T - 298) - 20.591 \times 10^3}{8.3144\,T}\right) \quad (3)$$

The parallel cathodic reactions of decomposition of the formed hydrogen peroxide, that may occur at the cathode, and described in Eqs.4 and 5 (Lim & Hoffmann, 2019), are limited by the carbon based material used as a cathode in the electrochemical cell.

$$H_2O_2 + H^+ + e^- \rightarrow H_2O + OH^- \quad (4)$$

$$H_2O_2 + 2H^+ + 2e^- \rightarrow 2H_2O \quad (5)$$

The possible reactions of formation or decomposition of hydrogen peroxide at the anode of the electrochemical cell are considered as very limited in acidic conditions, thus, the only pathway considered in the present paper in the cathodic one described earlier.

The electrochemical cell is energetically supplied by a continous current provided by a PV solar panel ET-Solar M53640 connected to a maximum power point tracker MPPT. The current I produced from the PV generator can be given by the Eq.6 (Villalva et al., 2009).

$$I = I_{pv} - I_d - I_{sh} \quad (6)$$

Where I_{pv} is the light-generated current of the PV cell I_d and I_{sh} are the current of the diode and current crossing shunt resistance, respectively (Rahim et al. 2015; Villalva, Gazoli, and Filho 2009). These parameters can be expressed through Eqs. 7, 8 and 9 (Rahim et al. 2015; Villalva et al., 2009):

$$I_{pv} = \frac{\left(I_{pv0} + K_I \Delta T\right)G}{G0} \quad (7)$$

$$I_d = I_0\left(\exp\left(\frac{R_s I + V}{V_t a}\right) - 1\right) \quad (8)$$

$$I_{sh} = \frac{V + R_s I}{R_p} \quad (9)$$

I_0 and ΔT are the diode saturation current and the variation in temperature at real and standard conditions that are given according Eqs. 10 and 11 (Villalva et al., 2009):

$$I_0 = \frac{I_{sc,n} + K_I \Delta T}{\exp\left(\frac{V_{ocn} + K_V \Delta T}{a V_t}\right) - 1} \quad (10)$$

$$\Delta T = T_p - T_n \quad (11)$$

Where V_{ocn}, K_I and K_V are the nominal open circuit voltage, current and voltage coefficient %/°C respectively. $I_{sc,n}$ is the nominal short circuit current and V_{tn}presents the thermal voltage at standard temperature and is given by Mohamed et al. (2016) in function of Boltzmann constant K_B, the charge of the electron q and the temperature at standard conditions T_n, as indicated in Eq.12.

$$V_{tn} = \frac{K_B T_n}{q} \quad (12)$$

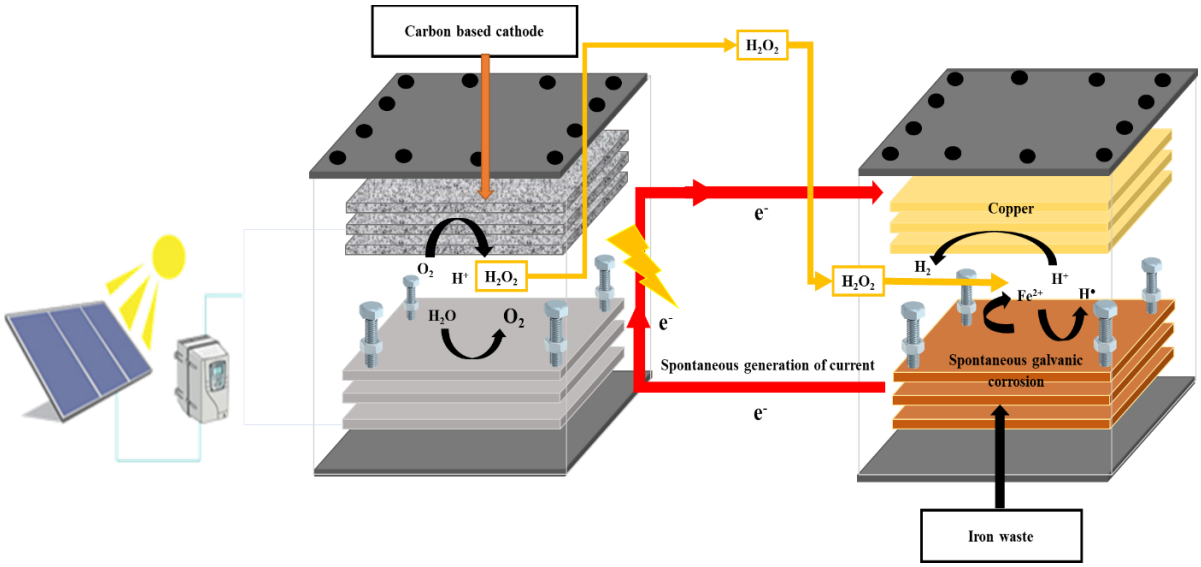

Figure 1. Galvanic cell for the spontaneous production of ferrous iron

Table 1. Specifications of the PV supplied electro-Galvano-Fenton process

	Parameter	Specification
Galvanic cell	Electrodes form	rectangular smooth plates
	Anode surface	12 cm^2
	Cathode surface	12 cm^2
	Anode material	Iron waste
	Cathode material	Copper
	Electrodes disposition	In parallel
Electrolyte	Electrolyte nature	Acidified water (H_2SO_4)
	Electrolyte volume	300 mL
	pH	3
	Electrical connection	External wire
	Ionic displacement	Aided by a magnetic stirring
Electrochemical cell	Initial concentration of hydrogen peroxide	0
	Cathode material	Carbon-based
	Anode material	Nickel
	Eelctrodes disposition	Parallel

In the Galvanic cell, the spontaneous corrosion of iron occurs under the effect of the higher redow potential of the couple (Cu^{2+}/Cu) constituting the cathode. The process is simulated considering a corrosion current of 300 µA, determined experimentally using A zero ammeter placed between both electrodes of the galvanic cell described in Table.1. The polarization curves have been also plotted using a galvanostat-potentiostat connected to the same cell, the corrosion current has been confirmed by this method as well, through the intersection of both Tafel's lines.

The current value is equivalent to a current density of 25 μA/cm^2 reported to the active surface of the anode of 12 cm^2. The Galvano-Fenton system is modeled by combining electrochemical reactions taking place at the anode and the cathode with chemical reactions related to the Fenton mechanism occurring in the bulk liquid volume. Table. 2 describes the whole evolution of the reactions occring at the electrodes and in the electrolyte.

Table 2. Electrochemical and chemical scheme of the possible reactions occurring at the electrodes and in the electrolyte by the integrated electrochemical and galvanic cells; k_i is the absolute reaction constant of the ith reaction. Adapted from electrolyte by the Sono-Galvano Fenton-based processes. k_i is the absolute reaction constant of the ith reaction. Adapted from Bray (1931) and Koprivanac & Lonˇ(2006) and De Laat & Le 2006 and Machulek et al. (2009).

	i	**ith Reaction**	**k_i**	**Unit of k_i**
Anode GC	1	$Fe \rightarrow Fe^{2+} + 2e^-$	-	-
Cathode GC	2	$2\,H^+ + 2e^- \rightarrow H_2$	-	-
Anode EC	3	$O_2 + 2\,H^+ + 2e^- \rightarrow H_2O_2$	-	-
	4	$Fe^{2+} + H_2O_2 \rightarrow Fe^{3+} + OH^- + HO^\bullet$	6.3×10^{-2}	$mol^{-1}.m^3.s^{-1}$
	5	$Fe^{3+} + H_2O_2 \rightarrow Fe(HO_2)^{2+} + H^+$	3.1×10^{4}	$mol^{-1}.m^3.s^{-1}$
	6	$Fe(HO_2)^{2+} + H^+ \rightarrow Fe^{3+} + H_2O_2$	1.0×10^{7}	$mol^{-1}.m^3.s^{-1}$
	7	$Fe(HO_2)^{2+} \rightarrow Fe^{2+} + HO_2^\bullet$	2.3×10^{-3}	s^{-1}
	8	$H_2O_2 + HO^\bullet \rightarrow HO_2^\bullet + H_2O$	3.3×10^{4}	$mol^{-1}.m^3.s^{-1}$
	9	$HO_2^\bullet \rightarrow O_2^{\bullet-} + H^+$	1.58×10^{5}	s^{-1}
	10	$O_2^{\bullet-} + H^+ \rightarrow HO_2^\bullet$	1.0×10^{7}	$mol^{-1}.m^3.s^{-1}$
	11	$Fe^{2+} + HO^\bullet \rightarrow Fe^{3+} + OH^-$	3.2×10^{5}	$mol^{-1}.m^3.s^{-1}$
	12	$HO_2^\bullet + Fe^{2+} + H_2O \rightarrow Fe^{3+} + H_2O_2 + OH^-$	1.2×10^{3}	$mol^{-1}.m^3.s^{-1}$
	13	$HO_2^\bullet + Fe^{3+} \rightarrow Fe^{2+} + H^+ + O_2$	3.6×10^{2}	$mol^{-1}.m^3.s^{-1}$
	14	$O_2^{\bullet-} + Fe^{2+} + 2H_2O \rightarrow Fe^{3+} + H_2O_2 + 2\,OH^-$	1.0×10^{4}	$mol^{-1}.m^3.s^{-1}$
	15	$O_2^{\bullet-} + Fe^{3+} \rightarrow Fe^{2+} + O_2$	5.0×10^{4}	$mol^{-1}.m^3.s^{-1}$
	16	$HO^\bullet + HO^\bullet \rightarrow H_2O_2$	5.2×10^{6}	$mol^{-1}.m^3.s^{-1}$
	17	$HO_2^\bullet + HO_2^\bullet \rightarrow H_2O_2 + O_2$	8.3×10^{2}	$mol^{-1}.m^3.s^{-1}$
	18	$O_2^{\bullet-} + H^+ \rightarrow HO_2^\bullet$	1.0×10^{7}	$mol^{-1}.m^3.s^{-1}$
	19	$HO^\bullet + HO_2^\bullet \rightarrow O_2 + H_2O$	7.1×10^{6}	$mol^{-1}.m^3.s^{-1}$
	20	$HO^\bullet + O_2^{\bullet-} \rightarrow O_2 + OH^-$	1.01×10^{7}	$mol^{-1}.m^3.s^{-1}$
Electrolyte	21	$HO_2^\bullet + O_2^{\bullet-} + H_2O \rightarrow H_2O_2 + O_2 + OH^-$	9.7×10^{4}	$mol^{-1}.m^3.s^{-1}$
	22	$HO_2^\bullet + H_2O_2 \rightarrow O_2 + HO^\bullet + H_2O$	5.0×10^{-4}	$mol^{-1}.m^3.s^{-1}$
	23	$O_2^{\bullet-} + H_2O_2 \rightarrow O_2 + HO^\bullet + OH^-$	1.3×10^{-4}	$mol^{-1}.m^3.s^{-1}$
	24	$Fe^{2+} + {SO_4}^{2-} \rightarrow FeSO_4$	2.29×10^{8}	$mol^{-1}.m^3.s^{-1}$
	25	${SO_4}^{2-} + HO^\bullet \rightarrow {SO_4}^{\bullet-} + OH^-$	1.4×10^{4}	$mol^{-1}.m^3.s^{-1}$
	26	${HSO_4}^- + HO^\bullet \rightarrow {SO_4}^{\bullet-} + H_2O$	3.5×10^{2}	$mol^{-1}.m^3.s^{-1}$
	27	${SO_4}^{\bullet-} + H_2O \rightarrow H^+ + {SO_4}^{2-} + HO^\bullet$	3.0×10^{5}	s^{-1}
	28	${SO_4}^{\bullet-} + OH^- \rightarrow {SO_4}^{2-} + HO^\bullet$	1.4×10^{4}	$mol^{-1}.m^3.s^{-1}$
	29	${SO_4}^{\bullet-} + H_2O_2 \rightarrow {SO_4}^{2-} + H^+ + HO_2^\bullet$	1.2×10^{4}	$mol^{-1}.m^3.s^{-1}$
	30	${SO_4}^{\bullet-} + HO_2^\bullet \rightarrow {SO_4}^{2-} + H^+ + O_2$	3.5×10^{6}	$mol^{-1}.m^3.s^{-1}$
	31	${SO_4}^{\bullet-} + Fe^{2+} \rightarrow Fe^{3+} + {SO_4}^{2-}$	3.0×10^{5}	$mol^{-1}.m^3.s^{-1}$
	32	$FeSO_4 \rightarrow Fe^{2+} + {SO_4}^{2-}$	1.0×10^{10}	s^{-1}
	33	$Fe^{3+} + H_2O \rightarrow FeOH^{2+} + H^+$	2.9×10^{7}	s^{-1}
	34	$FeOH^{2+} + H^+ \rightarrow Fe^{3+} + H_2O$	1.0×10^{7}	$mol^{-1}.m^3.s^{-1}$
	35	$FeOH^{2+} + H_2O_2 \rightarrow Fe(OH){HO_2}^+ + H^+$	2.0×10^{3}	$mol^{-1}.m^3.s^{-1}$
	36	$Fe(OH){HO_2}^+ + H^+ \rightarrow FeOH^{2+} + H_2O_2$	1.0×10^{7}	$mol^{-1}.m^3.s^{-1}$
	37	$Fe(OH){HO_2}^+ \rightarrow Fe^{2+} + HO_2^\bullet + OH^-$	2.3×10^{-3}	s^{-1}

Iron constitutes the sacrificial electrode in the galvanic cell, Fe oxidizes to Fe^{2+} (E^0 = −0.44 V vs. SHE) according to Equation 1, in Table.2. While at the cathode, the most probable reaction concerns the reduction of H^+ to form H_2 (E^0 = 0 V vs. SHE) according to Eq.2 in Table.2, owing to the acidity of the medium. This has been proven in a previous work conducted by our research group (Gasmi et al., 2020). The kinetics related to all of the electrochemical reactions are governed by Faraday's law (Ahmad, 2006), given in Eq.13, and describe the evolution of the C_k concentration of the species involved in the electrochemical reactions in a function of time.

$$\frac{dC_k}{dt} = \pm\frac{i_{corr}}{nFV} \tag{13}$$

n represents the valence number; it equals 2 for reaction 1 and 1 for reaction 2. F is Faraday's number, which equals 96,490 C/mol. i_{corr} represents the corrosion current, while V constitutes the volume of the electrolyte.

The chemical kinetic equations describing the evolution of the chemical mechanism occurring in the electrolyte are set based on the kinetics constant reported in previous table. Each reaction can be schematized according to Eq.14

$$\sum_{k=1}^{K} v'_{ki} X_k \rightarrow \sum_{k=1}^{K} v''_{ki} X_k \tag{14}$$

v'_{ki} is the stoichiometric coefficient related to the kth species X_k within the ith chemical reaction. The kinetics rate related to the i[th] reaction is expressed as reported in Eq.15.

$$r_i = k_i \prod_{k=1}^{K} [C_k]^{\vartheta' ki} \tag{151}$$

k_i is the kinetic constant related to the i^{th} reaction occurring in the electrolyte as reported in Table 2 and is determined at the operating temperature of 25 °C in the present study. The kinetics of apparition and the disappearance of a species X_k in the electrolyte is governed by Eq.16 for species involved in the electrochemical reactions:

$$\frac{d[X_k]}{dt} = \pm \frac{1}{nV} \frac{i_{corr}}{F} + \sum_{i=1}^{N} (v''_{ki} - v'_{ki})\, k_i \prod_{j=1}^{K} [X_j]^{\vartheta' ji} \tag{16}$$

While Eq.17 is applicable to species that are only implicated in the electrolytic reactions (Davis and Davis 2003).

$$\frac{d[X_k]}{dt} = \sum_{i=1}^{N} (v''_{ki} - v'_{ki})\, k_i \prod_{j=1}^{K} [X_j]^{\vartheta' ji} \tag{17}$$

The system of non-linear differential equations is resolved using the fourth-order Runge–Kutta algorithm with the function Ode 23s on Matlab with a fixed step of 1 s. The simulation is performed over 1500 s.

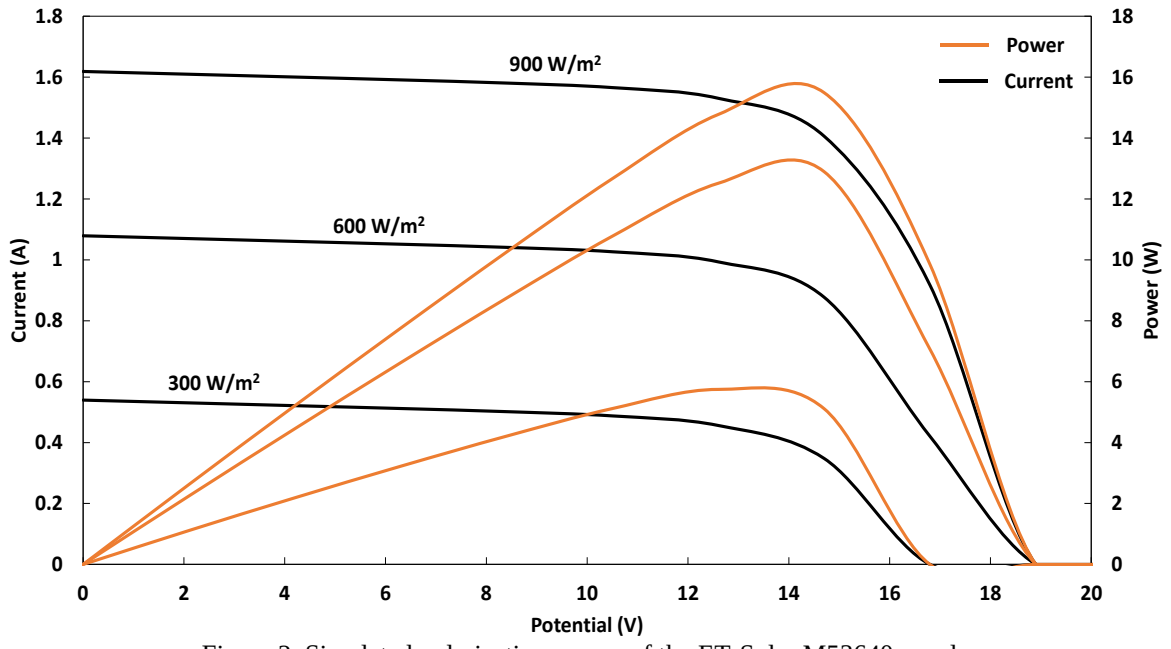

Figure 2. Simulated polarization curves of the ET-Solar M53640 panel

Results and Discussion

Performance of the PV Supply

The polarization curves of the studied solar panel have been simulated under three assumptions if incident global solar radiation, namely 300, 600 and 900 W/m^2. The highest values of deliverable power have been identified on the curves of the power vs. potential shown in Fig.2, they vary from 4.11 to 15.49 W when the solar radiation is increased from 300 to 900 W/m^2. The corresponding values of delivered current are then deduced from the curves of current vs. potential reported in the same figure, these values represent the feeding current of the electrochemical cell delivered by the MPPT regulator. The feeding current equals 0.35 A under 300 W/m^2, 0.88 A under 600 W/m^2 and finally 1.41 A under 900 W/m^2. These values are used in the model simulating the performance of the integrated process under the three studied situations.

Kinetics of Hydrogen Peroxide

The electrochemical in situ production of hydrogen peroxide is simulated according to the previous results and kinetics of hydrogen peroxide is reported in Fig.3 under the three scenarios of incident global solar radiation. As expected, the figure shows that the highest solar radiation leads to the highest production of hydrogen peroxide. A fraction of the produced hydrogen peroxide decomposes in the presence of ferrous ion, also produced in situ through the galvanic corrosion occurring in the integrated galvanic cell, Fig.3 depicts the evolution of the concentration of hydrogen peroxide as the result of the simultaneous in situ production and consumption in the Fenton reaction. After 1500 s, we can observe that the concentration of hydrogen peroxide attains 36.08 mol/m^3 under the highest solar radiation, i.e., 900 W/m^2. It equals 22.15 mol/m^3 under 600 W/m^2 and 8.69 mol/m^3 under 300 W/m^2. The availability of hydrogen peroxide in the solution reveals that the electrochemical technique produces in excess the Fenton's reagent, which is not actually in stoichiometric yields with the produced Fenton catalyst, suggesting to create parallel galvanic cells in order to augment the molar yield of ferrous ions and consume rapidly the produced hydrogen peroxide. This will be verified later in the section related to ferrous and ferric ions.

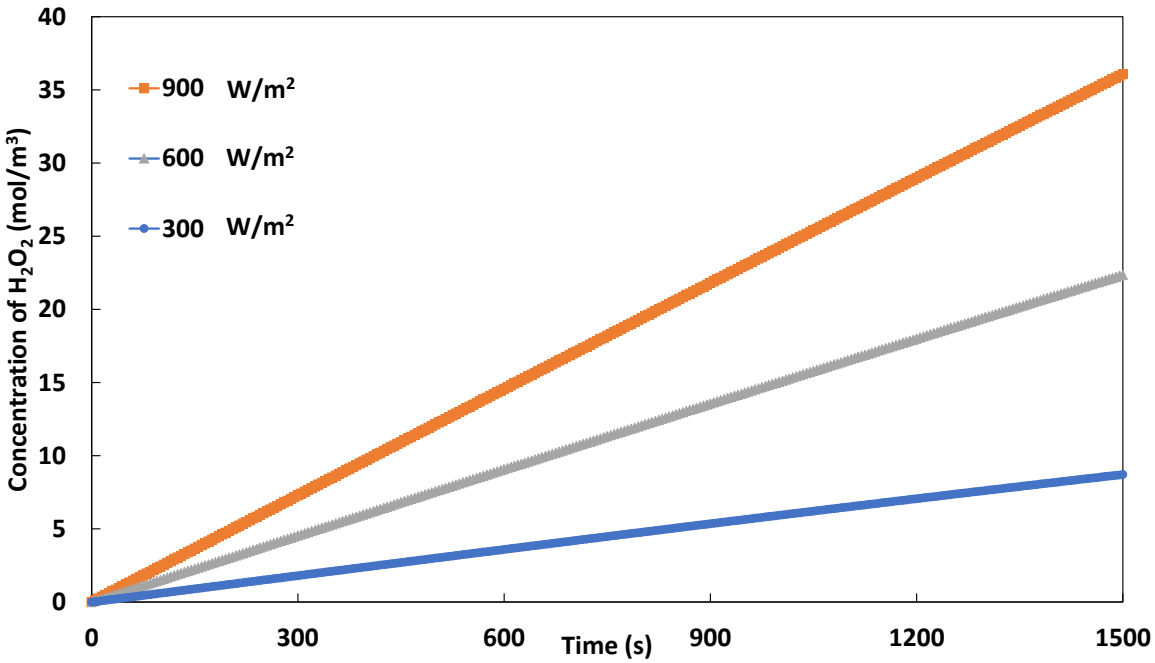

Figure 3. Evolutions of H_2O_2 concentration as a function of time under the different solar radiations

Kinetics of Ferrous and Ferric Ions

The simulated concentrations of ferrous and ferric ions are reported as function of time in Fig.4, according to the mechanism described in Table.2. interestingly, the highest solar radiation leads to the lowest concentrations of ferrous ions, revealing an important reactivity when hydrogen peroxide is available in higher molar yields. This

is verified with both other scenarios. However, the concentration of ferric ions does not follow the same trend, the values are almost the same with the three scenarios. This observation is probably explained by the slow regeneration of ferrous ions from ferric ions.

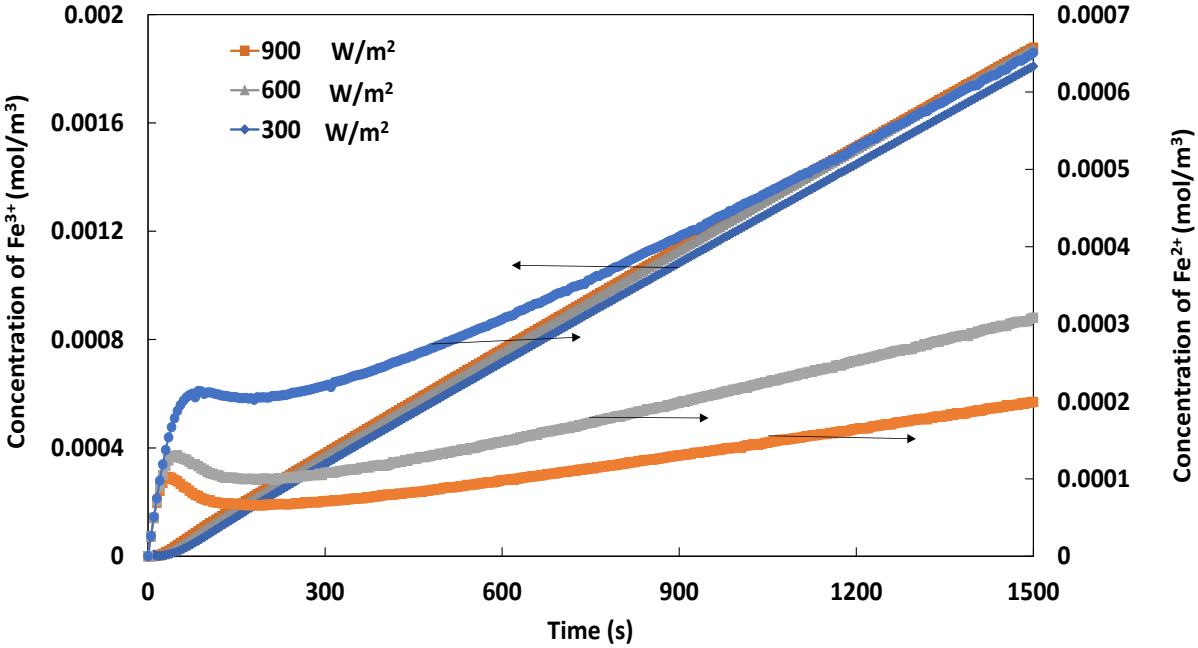

Figure 4. Evolution of the concentrations of ferric and ferrous ions as function of time under the different solar radiations.

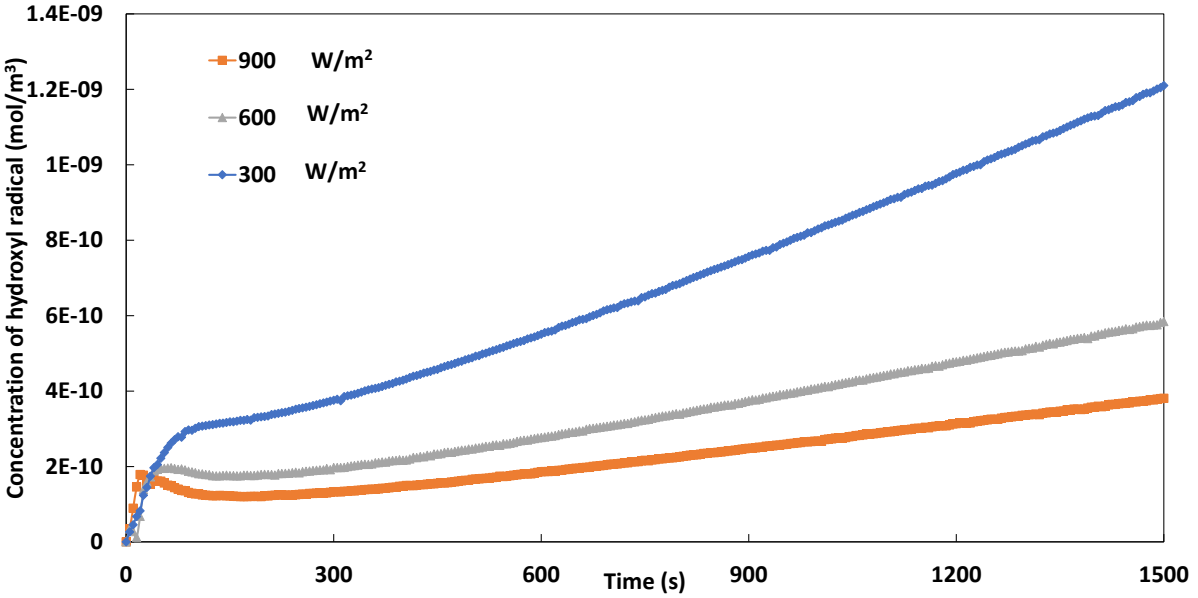

Figure 5. Evolution of the concentration of hydroxyl radical as a function of time under the different solar radiations

Production of Hydroxyl Radical

Fig. 5 reports the evolution of the concentration of hydroxyl radicals available in the electrolyte under the three scenarios of solar radiation. It is shown that the highest yield is observed under the lowest solar radiation, which confirms the unbalanced availability of hydrogen peroxide and ferrous ions leading to a rapid consumption of the catalyst and hence a braking in the instantaneous production of $HO^{\bullet}$. The lifetime of hydroxyl radicals being short, its rapid recombination leads to the emergence of hydrogen peroxide again in the medium, explain the higher concentrations observed under lower solar radiation, where the excess of hydrogen peroxide is

relatively reduced. This result confirms the need for parallel galvanic cells offering higher molar yields of ferrous ions, playing the role of catalyst in the decomposition if hydrogen peroxide, and making more efficient the proposed design of advanced oxidation process.

Conclusion

The PV supply of the electrochemical cell has been studied using modelling and simulation and the polariationcurves revealed that under 300, 600 and 900 W/m^2 of incident global solar radiation, the selected panel delivers 0.35, 0.88 and 1.41 A, respectively, according to the MPPT regulation. These current feeed the designed electrochemical cell, to intiaite the reducton of oxygen to hydrogen peroxide on a carbon based cathode, based on the assumption of a continous pumping of oxygen making the electrolyte permamently saturated. The simulations of the concentrations of hydrogen peroxide over time reveal that the electrochemical cell performs by far higher that the designed galvanic cell, suggesting to put several galvanic cells in parallel in order to reach stechiometric yields of Fenton's reagent and catalyst.

The trends retrieved with ferrous and ferric ions were interestingly unexpected. the highest solar radiation leads to the lowest concentrations of ferrous ions, revealing an important reactivity when hydrogen peroxide is available in higher molar yields. However, the concentration of ferric ions does not follow the same trend, the values are almost the same with the three scenarios, which is probably explained by the slow regeneration of ferrous ions from ferric ions. Similar trends were retrieved with hydroxyl radicals, which confirms the need for parallel galvanic cells offering higher molar yields of ferrous ions, playing the role of catalyst in the decomposition if hydrogen peroxide, and making more efficient the proposed design of advanced oxidation process.

Scientific Ethics Declaration

The author declares that the scientific ethical and legal responsibility of this article published in EPSTEM journal belongs to the author.

Acknowledgements or Notes

* This article was presented as an oral presentation at the International Conference on Technology (www.icontechno.net) conference held in Antalya/Turkey on November 16-19, 2023.

* This work was financially supported by the National Direction for Research and Technological Development DGRSDT, Algeria, in the frame of the "PISE" project entitled "GreEnAREA", supported by the mixed team of research "PVA" and affiliated to the National Higher School of Technology and Engineering.

References

Ahmad, Z.(2006). Corrosion kinetics. In B. T. Zaki (Ed.), *Principles of corrosion engineering and corrosion control Ahmad* (pp.57-119). Oxford: Butterworth-Heinemann.

Andreozzi, R., Antonio D Apuzzo, D. A., & Raffaele Marotta, R. (2000). A kinetic model for the degradation of benzothiazole by Fe3+ -photo-assisted fenton process in a completely mixed batch reactor. *Journal of Hazardous Materials*, *80*, 241–257.

Artusi, R., Verderio, P., & Marubini, E. (2002). Bravais-Pearson and Spearman correlation coefficients: Meaning, test of hypothesis and confidence interval. *International Journal of Biological Markers*, *17*(2), 148–151.

Bray, W.C. (1931). The mechanism of reactions in aqueous solution examples involving equilibria and steady states. *Chemical Reviews*, *1*, 161–77.

Davis, M. E., Robert, J., & Davis, R. J. (2003). The basics of reaction kinetics for chemical reaction engineering *Fundamentals of Chemical Reaction Engineering* (pp.1-52). New York, NY: McGraw Hill. Retrieved from http://resolver.caltech.edu.

De Laat, J., & Le, T.G. (2006). Effects of chloride ions on the iron(III)-catalyzed decomposition of hydrogen peroxide and on the efficiency of the fenton-like oxidation process. *Applied Catalysis B:*

Environmental, *66*(1–2), 137–146.

Gasmi, I. (2020). Kinetic pathways of iron electrode transformations in galvano-fnton process: A mechanistic investigation of in-situ catalyst formation and regeneration. *Journal of the Taiwan Institute of Chemical Engineers*, *116*, 81–91.

Haag, W. R. (1992). Rate constants for reaction of hydroxyl radicals with several drinking water contaminants. *Environmental Science and Technology*, *26*(5), 1005–1013.

Koprivanac, N., & Lonˇ, A. (2006). Photo-assisted fenton type processes for the degradation of phenol : A kinetic study. *Journal of Hazardous Materials*, *136*(3), 632–644.

Jonghun, L., & Hoffmann, M.R. (2019). Substrate oxidation enhances the electrochemical production of hydrogen peroxide. *Chemical Engineering Journal*, *374*, 958–64.

Machulek, A., de Moraes, J. E.F., & Okano, L.T.(2009). Photolysis of ferric ions in the presence of sulfate or chloride ions : Implications for the photo-fenton process." *Photochemical & Photobiological Sciences*, *8*, 985–991.

Madhavan, J., Grieser, F., & Ashokkumar, M. (2010). Combined advanced oxidation processes for the synergistic degradation of ibuprofen in aqueous environments. *Journal of Hazardous Materials*, *178*(1–3), 202–208.

Mohamed, B., Ali, B., Belasri, A., & Bouariou, A.(2016). Study of hydrogen production by solar energy as tool of storing and utilization renewable energy for the desert areas. *International Journal of Hydrogen Energy*, *41*(45), 20788–20806.

Pawar, V., & Gawande, S. (2015). An overview of the Fenton process for industrial wastewater. *IOSR Journal of Mechanical and Civil Engineering (IOSR-JMCE)*, 127–136.

Rahim, A. H., A. R., Tijani, A. S., Fadhullah, M., & Hanapi, S. (2015). Optimization of direct coupling solar PV panel and advanced alkaline electrolyzer system. *Energy, Procedia*, *79*, 204–211.

Tromans, D. (1998). Temperature and pressure dependent solubility of oxygen in water: A thermodynamic analysis. *Hydrometallurgy*, *48*(3), 327–342.

Villalva, M. G., Gazoli, J. R., & Filho, E. R.. (2009). Comprehensive approach to modeling and simulation of photovoltaic arrays. *IEEE Transactions on Power Electronics*, *24*(5), 1198–1208.

Author Information

Kaouther Kerboua
Department of Process and Energy Engineering.
National Higher School of Technology and Engineering,
23005, Annaba, Algeria
Contact e-mail: *k.kerboua@ensti-annaba.dz*

To cite this article:

Kerboua, K. (2023). PV supplied electrochemical production of hydrogen peroxide: Green pathway for Fenton based advanced oxidation processes. *The Eurasia Proceedings of Science, Technology, Engineering & Mathematics (EPSTEM), 24*, 101-109.